THE JOURNAL OF PHYSICAL CHEMISTRY LETTERS
A JOURNAL OF THE AMERICAN CHEMICAL SOCIETY

pubs.acs.org/JPCL

Letter

Influence of Fluorescence Lifetime Selections and Conformational Flexibility on Brightness of FusionRed Variants

Srijit Mukherjee, Nancy Douglas, and Ralph Jimenez*

Cite This: J. Phys. Chem. Lett. 2024, 15, 1644−1651

Read Online

ACCESS | Metrics & More | Article Recommendations | Supporting Information

ABSTRACT: Fluorescent proteins (FPs) for bioimaging are typically developed by screening mutant libraries for clones with improved photophysical properties. This approach has resulted in FPs with high brightness, but the mechanistic origins of the improvements are often unclear. We focused on improving the molecular brightness in the FusionRed family of FPs with fluorescence lifetime selections on targeted libraries, with the aim of reducing nonradiative decay rates. Our new variants show fluorescence quantum yields of up to 75% and lifetimes >3.5 ns. We present a comprehensive analysis of these new FPs, including trends in spectral shifts, photophysical data, photostability, and cellular brightness resulting from codon optimization. We also performed all-atom molecular dynamics simulations to investigate the impact of side chain mutations. The trajectories reveal that individual mutations reduce the flexibility of the chromophore and side chains, leading to an overall reduction in nonradiative rates.

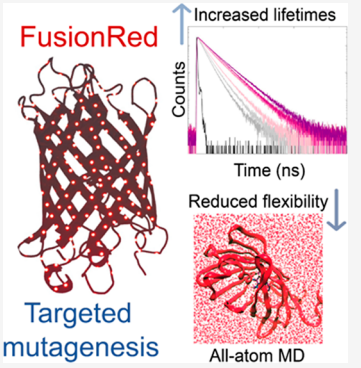

Fluorescent proteins (FPs) are commonly utilized as imaging probes and biosensors.[1,2] Despite the numerous advancements in engineering them over the past three decades, many FPs exhibit low brightness compared to synthetic organic fluorophores.[3] As a result, there is continued demand for improved variants, which are generally being developed by combining rational and random mutagenesis with high throughput screening.[4−11] Although the directed evolution approach has achieved notable success, it typically relies on repeated screenings of large mutant libraries, and the molecular basis for the outcomes is often unclear. For example, are any of the acquired mutations accidental, or are they all productive, and are molecular effects from individual mutations additive? These limitations may be overcome by integrating protein design principles based on quantitative, predictive, and generalizable concepts for protein function. Insights from crystallographic structures and spectroscopic studies have guided the rational design of FP libraries. However, the most frequently used selection methods such as fluorescence activated cell sorting (FACS) or microwell-based plate screening do not provide the detailed spectroscopic information obtained from in vitro studies.[12] As a result, selection efforts usually focus on only characterizing the final product. This approach leaves gaps in understanding intermediates from the directed evolution of photophysical properties. Higher information content screening methods, for example, based on fluorescence lifetime selections, have been introduced to address this limitation. These platforms have been employed to generate FPs with state-of-the-art brightness such as mScarlet, mTurquoise2, and mCherry-XL.[13−15] This approach has been successful because the fluorescence quantum yield for a closely related set of FPs, e.g., within a library, scales approximately linearly with lifetime, so the improved brightness is primarily due to decreased nonradiative decay rates.[16−19]

We recently combined lifetime-based selections with rational mutagenesis to develop brighter FusionRed (FR) variants, notably FR-MQV (FusionRed L175M, M42Q, C159V; ϕ = 0.53; τ = 2.8 ns), which is the brightest FR variant to date.[20] FR and its progeny are known for their high fidelity cellular localization and low toxicity,[21−23] utility in live-cell imaging, and gene expression studies.[21−24] Furthermore, the fluorescence blinking of FR variants at the single-molecule level has been utilized in super-resolution microscopy.[25−27] In the course of developing FR-MQV, we identified the M42Q mutation, which resulted in a significant increase (by ∼27%) in quantum yield and lifetime (by ∼20%). The inspiration to site-saturate this position in the sequence stemmed from our ultrafast spectroscopy studies on hydrogen bonding of the acylimine end of the chromophore in closely related FPs.[28] The L175M mutation in FR-MQV, selected through lifetime screening of libraries generated from error-prone mutagenesis, increased brightness in mammalian cells and extended the lifetime (by ∼20%).[29] Finally, the C159V mutation was obtained from lifetime screening of site-directed libraries

Received: October 4, 2023
Revised: January 14, 2024
Accepted: January 25, 2024
Published: February 5, 2024

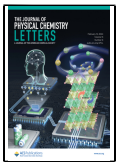

https://doi.org/10.1021/acs.jpclett.3c02765
J. Phys. Chem. Lett. 2024, 15, 1644−1651

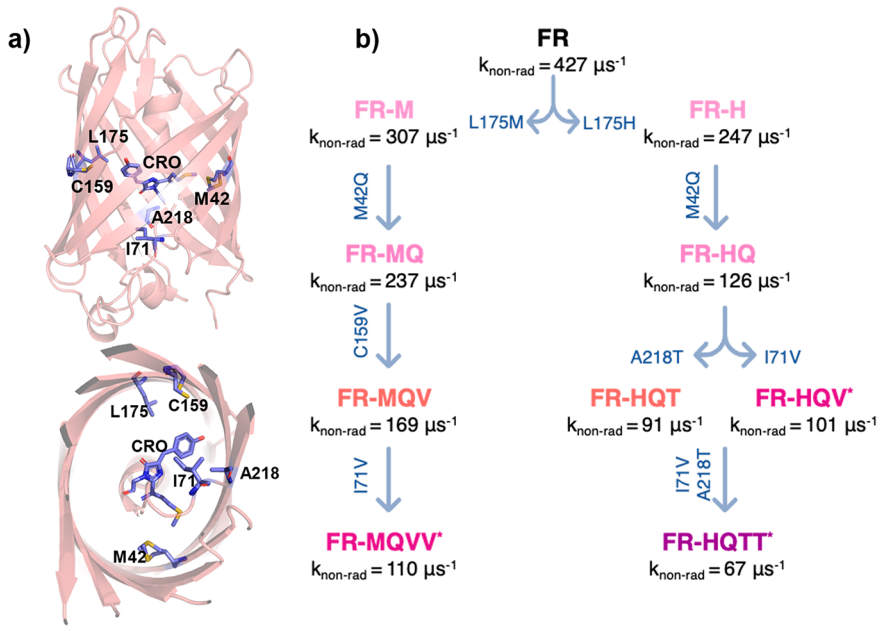

Figure 1. (a) Crystal structure of FusionRed (PDB code 6U1A) shown in top and side views, highlighting relevant mutations. The numbering corresponds to the convention employed in our previous study, offset by one compared to the PDB structure. (b) An evolutionary tree illustrates the sequence of mutations and the decrease in the nonradiative rate constants along the series.

targeting positions C159, M161, V196, and H198 based on the proximity of these residues to the phenol moiety of the RFP chromophore.[15] Despite these advances, no FR variants have been generated with quantum yields or lifetime that compare with mCherry-XL (ϕ = 0.70; τ = 3.9 ns) or mScarlet variants (ϕ > 0.70; τ = 3.9 ns), thus motivating further research into reducing its nonradiative rate.

Our goal in this study was to explore the mutational landscape of FR in search of variants with long fluorescence lifetimes and high quantum yields that rival mCherry-XL and mScarlet variants. We focused on reducing nonradiative rate using lifetime screening of individual bacterial colonies, sequence-position-targeted photophysical assessments, and all-atom molecular dynamics (MD) simulations. We surveyed the prospects for improvement beyond FR-MQV with brightness and lifetime flow cytometry on a FACS-enriched random mutagenesis library. We then sequentially targeted individual positions to evaluate the effects of substitutions. MD simulations provided insight into how the substitutions influence the conformational diversity of the chromophore environment. With this approach, and with only a few steps on the mutational manifold, we arrive at bright variants with quantum yields from 60% to 75%. A key finding of our study is that individual mutations leading to brighter FR variants consistently result in reduced conformational heterogeneity, corroborated by measured values of reduced nonradiative rate constants.

Mutagenesis. The quantum yield of molecular fluorescence may be expressed as a product of the radiative rate k_{rad} and the fluorescence lifetime τ, which in turn is related to the radiative and nonradiative $k_{non-rad}$ rate constants governing the depopulation of the excited state:[12]

$$\phi = k_{rad}\tau = \frac{k_{rad}}{k_{rad} + k_{non-rad}}$$

In general, values of k_{rad} and $k_{non-rad}$ can vary widely among molecular species.[12] However, for FPs we have shown (e.g., Figure 3 in ref 12 that values of k_{rad} vary modestly, whereas the values of $k_{non-rad}$ show much large variation. As a result, this expression implies that the fluorescence quantum yield of FPs is proportional to their lifetimes. The primary driver of high quantum yield in most FPs is their small values of $k_{non-rad}$.[12] For example, the radiative rate constant for FR-MQV (k_{rad} = 191 μs^{-1}) is comparable to that of bright FPs such as mScarlet3 (k_{rad} = 186 μs^{-1} and $k_{non-rad}$ = 72 μs^{-1}) and mCherry-XL (k_{rad} = 179 μs^{-1} and $k_{non-rad}$ = 76 μs^{-1}), but its value of $k_{non-rad}$ (169 μs^{-1}) is almost 2-fold larger.[13,15] We therefore evaluated the potential for the discovery of longer-lifetime FR-MQV variants that could translate to lower nonradiative rates and higher fluorescence quantum yields. First, random mutagenesis (i.e., error-prone PCR; EPPCR) was used to generate libraries with approximately 2, 4.5, and 16 mutations per kilobase at the nucleotide level. Libraries expressed in *E. coli* were enriched by FACS and screened for diversity in fluorescence lifetime (see Supporting Information Sections S1a and S2a for a detailed methodology). We consistently observed a wider distribution of fluorescence lifetime around the mean brightness of the parent FR-MQV in these libraries. The highest-error-rate EPPCR library exhibited a 1.25-fold higher variation in fluorescence lifetime compared to the lower error-rate libraries (Table S2.1). The diversity of the fluorescence lifetime in these libraries points to the existence of FR-MQV variants with longer lifetimes (details in Supporting Information Section S2a).

Next, we designed site-directed libraries at locations known to impact the FP photophysics but that were not thoroughly explored in the previous studies (see Figure 1 and Table 1). These small libraries of 20−400 variants were screened on plates to identify longer-lifetime variants (see Figure 2 and further details in Supporting Information Section S1d). Consequently, we performed saturation mutagenesis at position L175, which was previously identified as a position which led to photophysical diversity.[29] We observed that the L175H substitution resulted in a 1.3-fold increase in the

https://doi.org/10.1021/acs.jpclett.3c02765
J. Phys. Chem. Lett. 2024, 15, 1644−1651

Table 1. Amino Acid Substitutions for the FR Variants[a]

FP	42	71	159	175	218
FR	M	I	C	L	A
FR-Q	Q	I	C	L	A
FR-H	M	I	C	H	A
FR-M	M	I	C	M	A
FR-MQ	Q	I	C	M	A
FR-MQV	Q	I	V	M	A
FR-MQVV*	Q	V	V	M	A
FR-HQ	Q	I	C	H	A
FR-HQT	Q	I	C	H	T
FR-HQV*	Q	V	C	H	A
FR-HQTT*	Q	T	C	H	T

[a]The "*" denotes the amino acid at position 218.

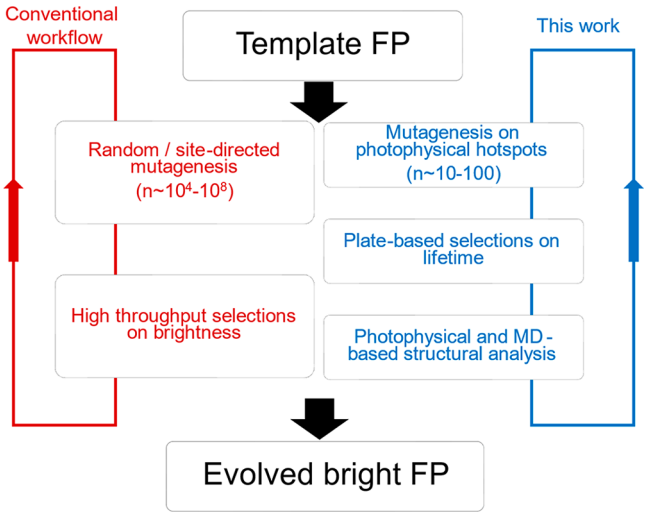

Figure 2. Comparison of workflows for FP development. Conventional FP engineering involves high throughput screening, in which the reliance of multiple, typically random mutations generates minimal new physical insights. Our approach employs small libraries with lifetime as a selection metric. In combination with photophysical and structural analyses, this methodology establishes fundamental principles related to molecular flexibility, which is shown to be the pivotal factor in enhancing fluorophore brightness.

fluorescence lifetime and a 1.8-fold increase in the quantum yield. We designate this variant "FR-H". We also found that amino acids with larger side chains, such as methionine (M), arginine (R), and histidine (H), extended the lifetime, whereas those with smaller side chains, such as serine (S), decreased it relative to FR (see Supporting Information Section S2b). Pursuing further mutagenesis at position 42 for FR-M and FR-H, the two variants with the longest lifetimes from the L175X library led to the rediscovery of M42Q as the substitution with the longest lifetime and highest quantum yield. Interestingly, FR-H M42Q (denoted "FR-HQ") had lifetime and quantum yield values exceeding FR-MQV ($\phi_{FR\text{-}MQV}$ = 0.53; $\tau_{FR\text{-}MQV}$ = 2.8 ns vs $\phi_{FR\text{-}HQ}$ = 0.60; $\tau_{FR\text{-}HQ}$ = 3.0 ns). Next, we performed saturation mutagenesis at position C159 on the two variants with the highest lifetime, FR-HQ and FR-MQ (details in Tables S23 and S2.4.). Lifetime screening confirmed that FR-HQ and FR-MQV are the brightest variants in these libraries.

Our next target for saturation was H198, which is analogous to R197 in mCherry-XL and T203 in the GFP variants.[15,30] Lin et al. have shown that chromophore interactions of superfolderGFP with T203 differentially stabilize the energies of the electronic resonance structures of the imidazolinone and phenolate rings by preferentially stabilizing the negative charge on the phenolate oxygen atom. This interaction impacts several aspects of the photophysics.[30] Based on this insight, we performed saturation mutagenesis at H198 in FR, FR-HQ, and FR-MQV and confirmed H198 to be a conserved mutation with respect to fluorescence, consistent with our prior observations.[20] Next, we reconsider a pathway for extended fluorescence lifetime discovered in the "FR-13" variant (FR: H23Y, V47I, F81Y and A218T).[29] In this case, the A218T mutation (designated as "FR-T") resulted in an increase in fluorescence lifetime and quantum yield compared to FR. Examination of the crystal structure of FR suggests that A218 can interact with H198 (see Supporting Information Figure S2.5). However, when we performed saturation mutagenesis at H198 on the FR-A218T variant, we found that H198 was the sole fluorescent variant in this library. Interestingly, A218 is also situated within hydrogen bonding distances to residues in the turn-region of the α-helix of FR, most notably I71. Mutations at this position have been explored in the development of the latest generation of bright FPs, e.g., mScarlet-I and mScarlet3.[13] Based on these observations, we performed saturation mutagenesis at positions A218 and I71 on FR-MQV and FR-HQ to generate a library of 400 variants. Lifetime screening of this library revealed several variants with lifetimes exceeding 3.5 ns and quantum yields of ≥65% (Supporting Information Table S2.5). Within the FR-H lineage, including FR-HQ I71V (designated as "FR-HQV*"), FR-HQ A218T (designated as "FR-HQT"), and FR-HQ A218T I71T (designated as "FR-HQTT*") and within the lineage of FR-MQV mutants, we discovered FR-MQV I71V (designated as "FR-MQVV*"). The spectra and lifetime decays of these variants are provided in Supporting Information Figure S3.1.

MD Simulations. We performed all-atom molecular dynamics simulations, spanning 500 ns,[31] to evaluate the influence of single substitutions at positions 175, 42, 159, and 218 in FR (Supporting Information Section S2). Computational details are provided in Supporting Information Section S1e. Simulations of the L175M variant (FR-M) revealed a single conformer of the side chain at position 175 situated approximately 1.5 Å closer to the chromophore, measured from the terminal heavy atom at position 175 to the methine bridge carbon on the chromophore. This finding substantiates the presence of a conformationally restricted environment proximal to the phenol moiety, as depicted in Supporting Information Figure S2.2. Similarly, the FR-M42Q substitution (FR-Q) led to a 60% reduction in conformational variability on the acylimine end, as probed by the distance between the chromophore acylimine oxygen and the side chain of Q42 (Supporting Information Figure S2.3). The trajectories reveal that interactions between side chains at positions 159 and 175 significantly decrease the conformational dynamics of both entities. The substitution C159V in the FR reduced the conformational heterogeneity of L175, thus mimicking the effect seen in the FR L175M substitution by itself. The reduced motion at position 175 leads to a less flexible chromophore interaction with C159 (Supporting Information Figure S2.4). The trajectories also suggest that the A218T mutation in FR creates a hydrogen bond with residue H198 (d_{DA} ~ 2 Å), also reducing the flexibility of this interaction (Supporting Information Figure S2.5).

https://doi.org/10.1021/acs.jpclett.3c02765
J. Phys. Chem. Lett. 2024, 15, 1644−1651

Table 2. Photophysical Data for the FR Variants and Other RFPs Discussed Here[a]

protein	$\lambda_{abs\ max}$ (nm)	$\lambda_{em\ max}$ (nm)	τ (ns)	ϕ (%)	ε_{max} (M^{-1} cm^{-1})	B (ε_{max}*ϕ)	k_{rad} (μs^{-1})	k_{nonrad} (μs^{-1})
FR	574	596	1.78 ± 0.03	24 ± 2	94000 ± 5500	100	135	427
FR-Q	567	587	2.11 ± 0.03	34 ± 3	133500 ± 7500	200	161	311
FR-M	571	591	2.15 ± 0.01	34 ± 1	75000 ± 6500	113	158	307
FR-MQ	567	586	2.45 ± 0.03	43 ± 2	129500 ± 5500	246	175	237
FR-MQV	566	585	2.78 ± 0.06	53 (ref)	141000 ± 9500	330	191	169
FR-MQVV*	565	582	3.37 ± 0.01	64 ± 1	96000 ± 6500	273	196	110
FR-H	568	588	2.34 ± 0.04	42 ± 3	120000 ± 4000	223	178	247
FR-HQ	565	583	3.17 ± 0.10	60 ± 1	118500 ± 10500	316	189	126
FR-HQT	566	583	3.50 ± 0.01	68 ± 2	65000 ± 15000	196	194	91
FR-HQV*	566	585	3.36 ± 0.05	66 ± 3	123500 ± 1500	360	196	101
FR-HQTT*	566	583	3.74 ± 0.04	75 ± 4	65500 ± 14000	218	200	67
mCherry	587	609	1.67 ± 0.07	22 (ref)	75500 ± 5000	75	137	488
mCherryXL	558	589	3.86 ± 0.05	70 ± 2	72000 ± 4000	223	179	76
mScarlet	569	592	3.87 ± 0.07	71 ± 2	104000 ± 4000	327	186	72

[a]Refer to Table 1 for sequences and Supporting Information (Sections S1 and S3) for methods and additional photophysical characterization.

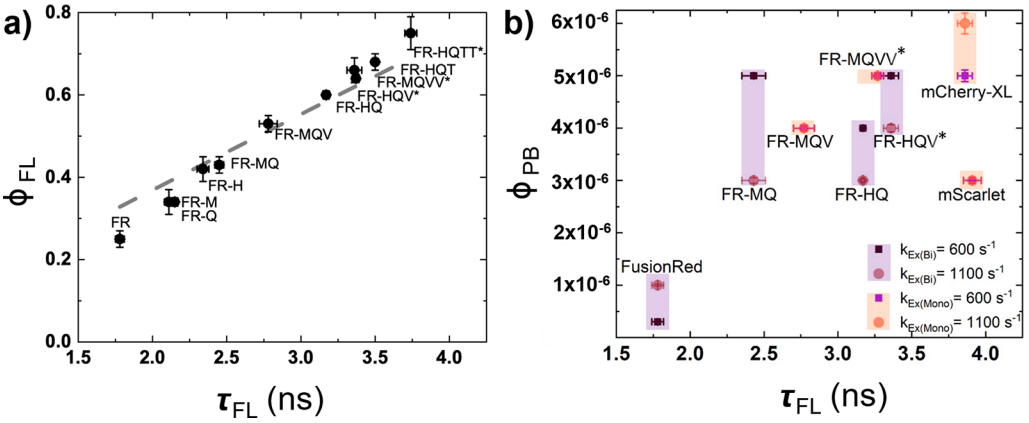

Figure 3. (a) A linear fit (y = 0.184 ± 0.004x, adj R^2 = 0.994)) of fluorescence quantum yield (ϕ_{FL}) versus fluorescence lifetime (τ_{FL}) for FR mutants. The slope of the line reflects the average radiative rate constant. A linear relationship indicates a near-constant radiative rate, where the reduction in the nonradiative rate drives the increase in fluorescence lifetime. (b) Quantum yield of photobleaching (ϕ_{PB}) versus fluorescence lifetime (τ_{FL}). FPs with dark state conversion (highlighted in purple) exhibit a reduced quantum yield of photobleaching due to the possible presence of photoprotective dark states. The photobleaching quantum yield values for FR-MQV, FR-MQVV*, and mScarlet are nearly the same at the two excitation rates (for mScarlet, the error bars in the measurement also overlap).

These mutations thus lead to reduced chromophore dynamics, as evidenced by the reduced chromophore RMSD values and reduced mean dihedral angles about the methine bridge (Supporting Information Section S4). For example, the heavy atom RMSD values for the individual mutants L175M, M42Q, C159V, and A218T are reduced 2-fold, 1.1-fold, 1.2-fold, and 2.4-fold, respectively, when compared to the template FR. These specific interactions, along with lower RMSD values for the chromophore in each of the individual mutations compared to the parental FP, indicate a more constrained chromophore in the ground state. These dynamics can in turn translate to higher rigidity in the excited state, which decreases the rate of nonradiative processes, e.g., associated with twisting of the methine bridge, and access to conical intersection (CI) seams as reported by Pieri et. al who examined access to CIs for variants of mScarlet and mRouge.[32] The effects observed in the trajectories of single mutants are additive, thus resulting in the longer lifetimes and higher quantum yields of brighter mutants such as FusionRed-MQVV*.

Photophysical Characterization. Properties of the relevant FPs are detailed in Table 2, and spectra and fluorescence lifetime decays are shown in Supporting Information Figure S3.1 (additional fit details and characterization in Supporting Information Section S3). The new FR variants show a near-linear correlation between the average fluorescence quantum yield and lifetime, as depicted in Figure 3a. For systems with multiexponential lifetime decays, when the multiple components are associated with the emission of multiple species with distinct radiative rates, the plot of fluorescence quantum yield vs lifetime is linear but it may show a nonzero intercept.[33] However, in this case, we interpret the high R^2 value for the linear fit with the fixed zero intercept to indicate that the average radiative rate of the FR variants does not vary significantly and that to a good approximation the mutations primarily suppress nonradiative pathways. We also find that across the 20−75% range of fluorescence quantum yield, the slope of the linear fit for FR variants is about 1.2 times larger than that for mCherry variants (Supporting Information, Figure S3.2b), which is consistent with the larger extinction coefficients for FR-variants. The finding that nonradiative rates consistently decrease with high quantum yield and lifetime, align with our results on mCherry and is further supported by the works of Lin et al. and Drobizhev et al. which utilized electronic Stark and two-photon excitation spectroscopy, respectively, to explore FP photophysics.[30,34] Long-lifetime FR variants show minimal shifts (~5 nm) in peak wavelengths

https://doi.org/10.1021/acs.jpclett.3c02765
J. Phys. Chem. Lett. 2024, 15, 1644−1651

and ∼10% changes in Stokes shifts (Supporting Information Figure S3.1). Note that the significant variation in the values of maximum extinction coefficient (ε_{max}) between bright mutants such as FR-MQVV* and FR-HQTT* is unexpected, given their very similar spectral features. These values were determined with the alkali denaturation method,[35] which is the most widely used assay. We used it here to obtain values consistent with the FP literature, although a previous study has reported that it generally overestimates the values of ε_{max}[35] (see Supporting Information Section S3c). For example, the nonradiative rate constant for FR-HQV* is almost the half of its precursor FR-HQ, but their absorption and emission spectra are identical. This observation supports our previous analysis of mCherry variants, where the change in the energy gap does not appear to be the primary driver for reducing nonradiative rates.[15] In this context, spectroscopic investigations to identify modes on the excited state manifold leading to ultrafast photoreactions may be insightful.[36] Interestingly, the M42Q mutation near the chromophore's acylimine end yields significant spectral changes (i.e., an absorption blue-shift of ∼215 cm^{-1} relative to FR), consistent with the findings of Moron et al. on the role of the acylimine dihedral angle in spectral shifts.[37] For variants of mCherry and mKate FPs, hydrogen-bonding interactions surrounding the acylimine end contribute to the far-red absorption and emission characteristics seen in FPs such as mPlum, mRojo, mNeptune, and TagRFP-675, albeit through different mechanisms.[38−42]

The maximum fluorescence quantum yield of 75% for FR-HQTT* is on par with those of the brightest RFPs such as mScarlet and mCherry-XL. Interestingly, in the latest generation of the mScarlet family, mScarlet3, the fluorescence quantum yield was only improved by 5%, with minimal spectral changes, despite significant advancements in chromophore maturation and cellular brightness.[13] This observation prompts questions about a potential theoretical limit for an RFP's MYG type-chromophore's fluorescence lifetime and quantum yield for a given absorption and emission spectra. Further exploration is needed to determine the origins of this apparent limit, whether it can be surpassed or is due to the interplay between the chromophore electronic structure and its interactions with the environment. Potentially, a Marcus−Hush-like analysis of charge separation between the oxygen atoms of the phenol, imidazolinone and the acylimine moieties of the RFP chromophore, analogous to the work of Lin et al., might unveil whether this trend could be due to a theoretical "saturation point".[30]

Photostability and Cellular Brightness. This study focused on the design of brighter FR variants by tuning conformational rigidity. However, from an application perspective, it is useful to assess the impact of the mutations on the properties of these FPs in cells. First, we assumed that the oligomerization of FusionRed remained uncompromised under the mutations acquired in this study. This assumption is grounded in our previous studies, where extensive oligomerization assays conclusively demonstrated that internal mutations seldom perturb the aggregation properties of FR.[20] However, we measured the photostability in bacteria and brightness in HeLa cells. We analyzed the photobleaching kinetics resulting from 561 nm widefield excitation normalized conditions at excitation rates of 600 s^{-1} and 1100 s^{-1} (corresponding to ∼7.5 and 15 W/cm^2 for FR). These FPs exhibit both monoexponential (FR V159 variants with mCherry-XL and mScarlet) and biexponential (FR C159 variants) decay kinetics, consistent with previous reports on FR variants (Figure S5.1).[20,26] Previously, we discovered that the biexponential decay kinetics associated with C159 result from reversible photobleaching mechanisms.[20] Rather than solely relying on the traditional method of assessing photobleaching, which involves determining the half-life based on the 50% intensity value of fluorescence decay at a given irradiance, we opted to fit the photobleaching traces to exponentials. In doing so, we used the resulting half-life values obtained from either the monoexponential trace or the longer component of the biexponential decay for these traces (Methodology detailed in Supporting Information Section S5). This analysis allowed for a quantitative comparative analysis of permanent photobleaching within the family of FR variants generated in this study.[12]

Our analysis indicates that dark state conversion is a photoprotective mechanism for FR-variants with biexponential bleaching kinetics. Variants with similar or longer lifetimes than FR-MQV but which exhibit biexponential photobleaching kinetics had a lower quantum yield of photobleaching (Figure 3b). At higher excitation rates, FPs such as FR-MQ, FR-HQ, and FR-HQV*, which have biexponential kinetics, show a reduction in the quantum yield of photobleaching (Figure 3b). This trend suggests that photostability is correlated with the propensity to convert to photoprotective (i.e., weakly absorbing) intermediate states. Investigations of the closely related FP TagRFP revealed that the nearly order of magnitude increase in photostability due to a S158T (equivalent to FR C159) mutation[43,44] can be explained with a "circular restoration model" based on insights from a crystallographic study of TagRFP which revealed the presence of both cis and trans fluorescent forms. In this model, conversion between protonated (nonfluorescent) and deprotonated (fluorescent) forms of the chromophore's cis and trans isomers comprises a photocycle which can "short-circuit" photobleaching in the S158T mutant but not in TagRFP.[45] Recently, QM/MM simulations confirmed that mutations at C159 can limit chromophore "I-twist" motion in the excited electronic state.[46] Accordingly, the C159V mutation in FR may limit the chromophore conformation to a single cis form facing S144, away from V159, thus blocking access to the "circular restoration" photocycle. This proposal is consistent with our observation that the C159V mutation impairs reversible photoswitching in FR, where multiexponential photobleaching kinetics at low irradiances (∼1−10 W/cm^2) are negligible (e.g., FR-MQVV*, mCherry, and mScarlet). These FPs may be more suitable for FRET-related applications in which dark state conversion is undesirable. However, this behavior can change significantly at higher excitation rates, which lead to shifts in the mechanisms of dark state conversion. Nevertheless, the significant observation here is that the creation of FPs with high molecular brightness is achievable without compromising the reversible photobleaching tendencies of the FP chromophore.

Expression in HeLa cells and the subsequent assessment of brightness were conducted using piggyBac-H2B vectors and flow cytometry, as detailed in Supporting Information Section S6. Our investigation aimed to quantify the cellular fluorescence brightness of three variants (FR-MQV, FR-MQVV*, and FR-HQV*) where chromophore maturation was not significantly diminished due to the incorporation of the A218T mutation. Human codon-optimized versions of the

https://doi.org/10.1021/acs.jpclett.3c02765
J. Phys. Chem. Lett. 2024, 15, 1644−1651

genes were purchased from a commercial gene synthesis company (Gene Universal, Newark, Delaware, USA), who use a proprietary algorithm for optimization. The codon-optimized versions of FR-MQVV and FR-HQV were 1.3-fold brighter compared to FR-MQV (mScarlet control). However, when compared to the non codon-optimized versions, we observed a significant drop in the brightness of codon-optimized FR-MQV. This result is unexpected, as codon optimization is expected to enhance protein expression levels. Furthermore, the counterintuitive nature of this result becomes even more pronounced when considering the minimal divergence in the codon composition between the variant and parent genes. This outcome underscores the complexity of predicting and interpreting the ramifications of codon optimization, particularly in cases where specific amino acid positions play a crucial role in protein structure and function.[47,48]

Outlook. To develop variants of FR with longer fluorescence lifetimes and higher brightness, we performed targeted mutagenesis at positions previously shown to produce photophysical diversity but which were not fully explored. In a series of library generations corroborated by MD simulations, we developed fluorophores with fluorescence quantum yields of up to 75%. This study aids in the general advancement of fluorescent tool development and provides insights into identifying key positions, such as A218 in FR, that are useful for reducing the nonradiative rates by increasing the rigidity of the chromophore environment. The chances of discovering and understanding the significance of these mutations would have been limited when using high-throughput evolution tools with low information content, such as FACS. These ideas extend beyond experimental principles, with the emergence of AI-assisted in silico methods such as AlphaFold and RosettaFold revolutionizing the design of synthetic proteins,[49,50] including FPs. Additionally, genetic code expansion, involving the incorporation of non-natural amino acids through engineered orthogonal translation systems in synthetic biology, presents a promising approach to creating a new generation of fluorescent tools driven by physical principles of reduced conformational space and ideal positioning indices for key residues around fluorescent chromophores.[51] Future efforts combining these methods could potentially generate new fluorophores, surpassing the performance of the best currently available FPs.

■ ASSOCIATED CONTENT

Supporting Information

The Supporting Information is available free of charge at https://pubs.acs.org/doi/10.1021/acs.jpclett.3c02765.

Section S1 on the methods and materials used for the data presented in the study; Section S2 covering the protocols for library generation and the strategy for recognizing photophysical "hotspots"; Sections S3 and S4 providing additional photophysical data and the results of MD simulations, respectively; Section S5 discussing photostability; Section S6 describing cellular brightness assays (PDF)

■ AUTHOR INFORMATION

Corresponding Author

Ralph Jimenez − *JILA, University of Colorado, Boulder, and National Institute of Standards and Technology, Boulder, Colorado 80309, United States; Department of Chemistry, University of Colorado, Boulder, Boulder, Colorado 80309, United States;* orcid.org/0000-0002-8989-405X; Email: rjimenez@jila.colorado.edu

Authors

Srijit Mukherjee − *JILA, University of Colorado, Boulder, and National Institute of Standards and Technology, Boulder, Colorado 80309, United States; Department of Chemistry, University of Colorado, Boulder, Boulder, Colorado 80309, United States; Department of Chemistry, Stanford University, Stanford, California 94305, United States;* orcid.org/0000-0002-6439-9802

Nancy Douglas − *Department of Chemistry, University of Colorado, Boulder, Boulder, Colorado 80309, United States*

Complete contact information is available at: https://pubs.acs.org/10.1021/acs.jpclett.3c02765

Author Contributions

S.M. and R.J. conceptualized the study. S.M. and N.D. designed and performed the experiments. R.J. and S.M. designed and analyzed the simulations. S.M. and R.J. developed data analysis methods in the study. S.M., N.D., and R.J. wrote the manuscript.

Notes

The authors declare no competing financial interest.

■ ACKNOWLEDGMENTS

S.M. was supported by the NIH/CU Molecular Biophysics Training Program (Grant T32). This work was partially supported by the NSF Physics Frontier Center at JILA (Grant PHY 2317149 to R.J.). R.J. is a member of the Quantum Physics Division of the National Institute of Standards and Technology (NIST). Certain commercial equipment, instruments, or materials are identified in this paper in order to specify the experimental procedure adequately. Such identification is not intended to imply recommendation or endorsement by the NIST, nor is it intended to imply that the materials or equipment identified are necessarily the best available for the purpose. Spectroscopy was performed at the W. M. Keck Optical Measurements Laboratory in JILA. We acknowledge Theresa Nahreini and the Flow Cytometry shared core facility at BioFrontiers Institute, CU Boulder (supported by Grant NIH S10ODO21601). Finally, we also thank Prof. Amy E. Palmer, Prof. Prem P. Chapagain, Prof. ShengTing Hung, Dr. Premashis Manna, and Jacob Kirsh for valuable discussions.

■ REFERENCES

(1) Tsien, R. Y. The Green Fluorescent Protein. *Annu. Rev. Biochem.* **1998**, *67* (1), 509−544.

(2) Shaner, N. C.; Steinbach, P. A.; Tsien, R. Y. A Guide to Choosing Fluorescent Proteins. *Nat. Methods* **2005**, *2* (12), 905−909.

(3) Lambert, T. J. FPbase: A Community-Editable Fluorescent Protein Database. *Nature Methods.* **2019**, *16*, 277−278.

(4) Ai, H. W.; Baird, M. A.; Shen, Y.; Davidson, M. W.; Campbell, R. E. Engineering and Characterizing Monomeric Fluorescent Proteins for Live-Cell Imaging Applications. *Nat. Protoc.* **2014**, *9* (4), 910−928.

(5) Truong, L.; Ferré-D'Amaré, A. R. From Fluorescent Proteins to Fluorogenic RNAs: Tools for Imaging Cellular Macromolecules. *Protein Sci.* **2019**, *28* (8), 1374−1386.

(6) Campbell, B. C.; Paez-Segala, M. G.; Looger, L. L.; Petsko, G. A.; Liu, C. F. Chemically Stable Fluorescent Proteins for Advanced Microscopy. *Nat. Methods* **2022**, *19* (12), 1612−1621.

(7) Bindels, D. S.; Haarbosch, L.; Van Weeren, L.; Postma, M.; Wiese, K. E.; Mastop, M.; Aumonier, S.; Gotthard, G.; Royant, A.; Hink, M. A.; Gadella, T. W. J. MScarlet: A Bright Monomeric Red Fluorescent Protein for Cellular Imaging. *Nat. Methods* **2017**, *14* (1), 53−56.
(8) Legault, S.; Fraser-Halberg, D. P.; McAnelly, R. L.; Eason, M. G.; Thompson, M. C.; Chica, R. A. Generation of Bright Monomeric Red Fluorescent Proteins via Computational Design of Enhanced Chromophore Packing. *Chem. Sci.* **2022**, *13* (5), 1408−1418.
(9) Lambert, G. G.; Depernet, H.; Gotthard, G.; Schultz, D. T.; Navizet, I.; Lambert, T.; Adams, S. R.; Torreblanca-Zanca, A.; Chu, M.; Bindels, D. S.; Levesque, V.; Moffatt, J. N.; Salih, A.; Royant, A.; Shaner, N. C. Aequorea's Secrets Revealed: New Fluorescent Proteins with Unique Properties for Bioimaging and Biosensing. *PLoS Biol.* **2020**, *18* (11), e3000936.
(10) Campbell, B. C.; Nabel, E. M.; Murdock, M. H.; Lao-Peregrin, C.; Tsoulfas, P.; Blackmore, M. G.; Lee, F. S.; Liston, C.; Morishita, H.; Petsko, G. A. mGreenLantern: A Bright Monomeric Fluorescent Protein with Rapid Expression and Cell Filling Properties for Neuronal Imaging. *Proc. Natl. Acad. Sci. U. S. A.* **2020**, *117* (48), 30710−30721.
(11) Hirano, M.; Ando, R.; Shimozono, S.; Sugiyama, M.; Takeda, N.; Kurokawa, H.; Deguchi, R.; Endo, K.; Haga, K.; Takai-Todaka, R.; Inaura, S.; Matsumura, Y.; Hama, H.; Okada, Y.; Fujiwara, T.; Morimoto, T.; Katayama, K.; Miyawaki, A. A Highly Photostable and Bright Green Fluorescent Protein. *Nat. Biotechnol.* **2022**, *40* (7), 1132−1142.
(12) Mukherjee, S.; Jimenez, R. Photophysical Engineering of Fluorescent Proteins: Accomplishments and Challenges of Physical Chemistry Strategies. *J. Phys. Chem. B* **2022**, *126* (4), 735−750.
(13) Gadella, T. W. J.; van Weeren, L.; Stouthamer, J.; Hink, M. A.; Wolters, A. H. G.; Giepmans, B. N. G.; Aumonier, S.; Dupuy, J.; Royant, A. mScarlet3: A Brilliant and Fast-Maturing Red Fluorescent Protein. *Nat. Methods* **2023**, *20* (4), 541−545.
(14) Goedhart, J.; Von Stetten, D.; Noirclerc-Savoye, M.; Lelimousin, M.; Joosen, L.; Hink, M. A.; Van Weeren, L.; Gadella, T. W. J.; Royant, A. Structure-Guided Evolution of Cyan Fluorescent Proteins towards a Quantum Yield of 93%. *Nat. Commun.* **2012**, *3*, 3.
(15) Mukherjee, S.; Manna, P.; Hung, S. T.; Vietmeyer, F.; Friis, P.; Palmer, A. E.; Jimenez, R. Directed Evolution of a Bright Variant of MCherry: Suppression of Nonradiative Decay by Fluorescence Lifetime Selections. *J. Phys. Chem. B* **2022**, *126* (25), 4659−4668.
(16) Dean, K. M.; Lubbeck, J. L.; Davis, L. M.; Regmi, C. K.; Chapagain, P. P.; Gerstman, B. S.; Jimenez, R.; Palmer, A. E. Microfluidics-Based Selection of Red-Fluorescent Proteins with Decreased Rates of Photobleaching. *Integr. Biol. (United Kingdom)* **2015**, *7* (2), 263−273.
(17) Dean, K. M.; Davis, L. M.; Lubbeck, J. L.; Manna, P.; Friis, P.; Palmer, A. E.; Jimenez, R. High-Speed Multiparameter Photophysical Analyses of Fluorophore Libraries. *Anal. Chem.* **2015**, *87* (10), 5026−5030.
(18) Hung, S. T.; Mukherjee, S.; Jimenez, R. Enrichment of Rare Events Using a Multi-Parameter High Throughput Microfluidic Droplet Sorter. *Lab Chip* **2020**, *20* (4), 834−843.
(19) Bindels, D. S.; Postma, M.; Haarbosch, L.; van Weeren, L.; Gadella, T. W. J. Multiparameter Screening Method for Developing Optimized Red-Fluorescent Proteins. *Nat. Protoc.* **2020**, *15* (2), 450−478.
(20) Mukherjee, S.; Hung, S. T.; Douglas, N.; Manna, P.; Thomas, C.; Ekrem, A.; Palmer, A. E.; Jimenez, R. Engineering of a Brighter Variant of the FusionRed Fluorescent Protein Using Lifetime Flow Cytometry and Structure-Guided Mutations. *Biochemistry* **2020**, *59* (39), 3669−3682.
(21) Shemiakina, I. I.; Ermakova, G. V.; Cranfill, P. J.; Baird, M. A.; Evans, R. A.; Souslova, E. A.; Staroverov, D. B.; Gorokhovatsky, A. Y.; Putintseva, E. V.; Gorodnicheva, T. V.; Chepurnykh, T. V.; Strukova, L.; Lukyanov, S.; Zaraisky, A. G.; Davidson, M. W.; Chudakov, D. M.; Shcherbo, D. A Monomeric Red Fluorescent Protein with Low Cytotoxicity. *Nat. Commun.* **2012**, *3*, 1204.
(22) Yoon, S.; Pan, Y.; Shung, K.; Wang, Y. FRET-Based Ca2+ Biosensor Single Cell Imaging Interrogated by High-Frequency Ultrasound. *Sensors* **2020**, *20* (17), 4998.
(23) Chernov, K. G.; Manoilov, K. Y.; Oliinyk, O. S.; Shcherbakova, D. M.; Verkhusha, V. V. Photodegradable by Yellow-Orange Light DegFusionRed Optogenetic Module with Autocatalytically Formed Chromophore. *Int. J. Mol. Sci.* **2023**, *24* (7), 6526.
(24) Muslinkina, L.; Pletnev, V. Z.; Pletneva, N. V.; Ruchkin, D. A.; Kolesov, D. V.; Bogdanov, A. M.; Kost, L. A.; Rakitina, T. V.; Agapova, Y. K.; Shemyakina, I. I.; Chudakov, D. M.; Pletnev, S. Two Independent Routes of Post-Translational Chemistry in Fluorescent Protein FusionRed. *Int. J. Biol. Macromol.* **2020**, *155*, 551−559.
(25) Pennacchietti, F.; Serebrovskaya, E. O.; Faro, A. R.; Shemyakina, I. I.; Bozhanova, N. G.; Kotlobay, A. A.; Gurskaya, N. G.; Bodén, A.; Dreier, J.; Chudakov, D. M.; Lukyanov, K. A.; Verkhusha, V. V.; Mishin, A. S.; Testa, I. Fast Reversibly Photoswitching Red Fluorescent Proteins for Live-Cell RESOLFT Nanoscopy. *Nat. Methods* **2018**, *15* (8), 601−604.
(26) Mukherjee, S.; Thomas, C.; Wilson, R.; Simmerman, E.; Hung, S. T.; Jimenez, R. Characterizing Dark State Kinetics and Single Molecule Fluorescence of FusionRed and FusionRed-MQ at Low Irradiances. *Phys. Chem. Chem. Phys.* **2022**, *24* (23), 14310−14323.
(27) Klementieva, N. V.; Pavlikov, A. I.; Moiseev, A. A.; Bozhanova, N. G.; Mishina, N. M.; Lukyanov, S. A.; Zagaynova, E. V.; Lukyanov, K. A.; Mishin, A. S. Intrinsic Blinking of Red Fluorescent Proteins for Super-Resolution Microscopy. *Chem. Commun.* **2017**, *53* (5), 949−951.
(28) Yoon, E.; Konold, P. E.; Lee, J.; Joo, T.; Jimenez, R. Far-Red Emission of MPlum Fluorescent Protein Results from Excited-State Interconversion between Chromophore Hydrogen-Bonding States. *J. Phys. Chem. Lett.* **2016**, *7* (12), 2170−2174.
(29) Manna, P.; Hung, S. T.; Mukherjee, S.; Friis, P.; Simpson, D. M.; Lo, M. N.; Palmer, A. E.; Jimenez, R. Directed Evolution of Excited State Lifetime and Brightness in FusionRed Using a Microfluidic Sorter. *Integr. Biol. (United Kingdom)* **2018**, *10* (9), 516−526.
(30) Lin, C. Y.; Romei, M. G.; Oltrogge, L. M.; Mathews, I. I.; Boxer, S. G. Unified Model for Photophysical and Electro-Optical Properties of Green Fluorescent Proteins. *J. Am. Chem. Soc.* **2019**, *141* (38), 15250−15265.
(31) Mukherjee, S.; Manna, P.; Douglas, N.; Chapagain, P. P.; Jimenez, R. Conformational Dynamics of mCherry Variants: A Link between Side-Chain Motions and Fluorescence Brightness. *J. Phys. Chem. B* **2023**, *127* (1), 52−61.
(32) Pieri, E.; Walker, A. R.; Zhu, M.; Martínez, T. J. Conical Intersection Accessibility Dictates Brightness in Red Fluorescent Proteins. *ChemRxiv* **2023**, DOI: 10.26434/chemrxiv-2023-xn5l3.
(33) Sillen, A.; Engelborghs, Y. The Correct Use of "Average" Fluorescence Parameters. *Photochem. Photobiol.* **1998**, *67* (5), 475−486.
(34) Drobizhev, M.; Molina, R. S.; Callis, P. R.; Scott, J. N.; Lambert, G. G.; Salih, A.; Shaner, N. C.; Hughes, T. E. Local Electric Field Controls Fluorescence Quantum Yield of Red and Far-Red Fluorescent Proteins. *Front. Mol. Biosci.* **2021**, *8*, 633217.
(35) Kredel, S.; Nienhaus, K.; Oswald, F.; Wolff, M.; Ivanchenko, S.; Cymer, F.; Jeromin, A.; Michel, F. J.; Spindler, K. D.; Heilker, R.; Nienhaus, G. U.; Wiedenmann, J. Optimized and Far Red-Emitting Variants of Fluorescent Protein EqFP611. *Chem. Biol.* **2008**, *15* (3), 224−233.
(36) Chen, C.; Henderson, J. N.; Ruchkin, D. A.; Kirsh, J. M.; Baranov, M. S.; Bogdanov, A. M.; Mills, J. H.; Boxer, S. G.; Fang, C. Structural Characterization of Fluorescent Proteins Using Tunable Femtosecond Stimulated Raman Spectroscopy. *Int. J. Mol. Sci.* **2023**, *24*, 11991.
(37) Moron, V.; Marazzi, M.; Wanko, M. Far Red Fluorescent Proteins: Where Is the Limit of the Acylimine Chromophore? *J. Chem. Theory Comput.* **2019**, *15* (7), 4228−4240.

https://doi.org/10.1021/acs.jpclett.3c02765
J. Phys. Chem. Lett. 2024, 15, 1644−1651

(38) Abbyad, P.; Childs, W.; Shi, X.; Boxer, S. G. Dynamic Stokes Shift in Green Fluorescent Protein Variants. *Proc. Natl. Acad. Sci. U. S. A.* **2007**, *104* (51), 20189−20194.
(39) Konold, P.; Regmi, C. K.; Chapagain, P. P.; Gerstman, B. S.; Jimenez, R. Hydrogen Bond Flexibility Correlates with Stokes Shift in mPlum Variants. *J. Phys. Chem. B* **2014**, *118* (11), 2940−2948.
(40) Faraji, S.; Krylov, A. I. On the Nature of an Extended Stokes Shift in the mPlum Fluorescent Protein. *J. Phys. Chem. B* **2015**, *119* (41), 13052−13062.
(41) Yoon, E.; Konold, P. E.; Lee, J.; Joo, T.; Jimenez, R. Far-Red Emission of mPlum Fluorescent Protein Results from Excited-State Interconversion between Chromophore Hydrogen-Bonding States. *J. Phys. Chem. Lett.* **2016**, *7* (12), 2170−2174.
(42) Chica, R. A.; Moore, M. M.; Allen, B. D.; Mayo, S. L. Generation of Longer Emission Wavelength Red Fluorescent Proteins Using Computationally Designed Libraries. *Proc. Natl. Acad. Sci. U. S. A.* **2010**, *107* (47), 20257−20262.
(43) Shaner, N. C.; Lin, M. Z.; McKeown, M. R.; Steinbach, P. A.; Hazelwood, K. L.; Davidson, M. W.; Tsien, R. Y. Improving the Photostability of Bright Monomeric Orange and Red Fluorescent Proteins. *Nat. Methods* **2008**, *5* (6), 545−551.
(44) Dean, K. M.; Lubbeck, J. L.; Binder, J. K.; Schwall, L. R.; Jimenez, R.; Palmer, A. E. Analysis of Red-Fluorescent Proteins Provides Insight into Dark-State Conversion and Photodegradation. *Biophys. J.* **2011**, *101* (4), 961−969.
(45) Liu, R.; Liang, Q. N.; Du, S. Q.; Hu, X. J.; Ding, Y. The Crystal Structure of Red Fluorescent Protein TagRFP-T Reveals the Mechanism of Its Superior Photostability. *Biochem. Biophys. Res. Commun.* **2016**, *477* (2), 229−234.
(46) Murphy, A. R.; Hix, M. A.; Walker, A. Exploring the Effects of Mutagenesis on FusionRed Using Excited State QM/MM Dynamics and Classical Force Field Simulations. *ChemBioChem* **2023**, *24* (12), No. e202200799.
(47) Ranaghan, M. J.; Li, J. J.; Laprise, D. M.; Garvie, C. W. Assessing Optimal: Inequalities in Codon Optimization Algorithms. *BMC Biol.* **2021**, *19* (1), 36.
(48) Mauro, V. P.; Chappell, S. A. A Critical Analysis of Codon Optimization in Human Therapeutics. *Trends Mol. Med.* **2014**, *20* (11), 604−613.
(49) Jumper, J.; Evans, R.; Pritzel, A.; Green, T.; Figurnov, M.; Ronneberger, O.; Tunyasuvunakool, K.; Bates, R.; Žídek, A.; Potapenko, A.; Bridgland, A.; Meyer, C.; Kohl, S. A. A.; Ballard, A. J.; Cowie, A.; Romera-Paredes, B.; Nikolov, S.; Jain, R.; Adler, J.; Back, T.; Petersen, S.; Reiman, D.; Clancy, E.; Zielinski, M.; Steinegger, M.; Pacholska, M.; Berghammer, T.; Bodenstein, S.; Silver, D.; Vinyals, O.; Senior, A. W.; Kavukcuoglu, K.; Kohli, P.; Hassabis, D. Highly Accurate Protein Structure Prediction with AlphaFold. *Nature* **2021**, *596* (7873), 583−589.
(50) Baek, M.; DiMaio, F.; Anishchenko, I.; Dauparas, J.; Ovchinnikov, S.; Lee, G. R.; Wang, J.; Cong, Q.; Kinch, L. N.; Schaeffer, R. D.; Millán, C.; Park, H.; Adams, C.; Glassman, C. R.; DeGiovanni, A.; Pereira, J. H.; Rodrigues, A. V.; Van Dijk, A. A.; Ebrecht, A. C.; Opperman, D. J.; Sagmeister, T.; Buhlheller, C.; Pavkov-Keller, T.; Rathinaswamy, M. K.; Dalwadi, U.; Yip, C. K.; Burke, J. E.; Garcia, K. C.; Grishin, N. V.; Adams, P. D.; Read, R. J.; Baker, D. Accurate Prediction of Protein Structures and Interactions Using a Three-Track Neural Network. *Science* **2021**, *373* (6557), 871−876.
(51) Link, A. J.; Mock, M. L.; Tirrell, D. A. Non-Canonical Amino Acids in Protein Engineering. *Curr. Opin. Biotechnol.* **2003**, *14* (6), 603−609.

https://doi.org/10.1021/acs.jpclett.3c02765
J. Phys. Chem. Lett. 2024, 15, 1644−1651